Adsorption in Single-Walled Carbon Nanotubes by Experiments and Molecular Simulation I: Determining Fraction of Open-ended Nanotubes in Samples

Sandeep Agnihotri,[1] Jose' P. B. Mota,[2] Massoud Rostam-Abadi,[3,4] Mark. J. Rood[4]

[1]Department of Civil and Environmental Engineering, University of Tennessee, Knoxville. sagnihot@utk.edu; [2]Requimte/CQFB, Departamento de Quimica, Faculdade de Ciencias e Tecnologia, Univerdade Nova de Lisboa, 2829-516, Caparica, Portugal pmota@dq.fct.unl.pt; [3]Illinois State Geological Survey, 615 E Peabody Dr., Champaign IL massoud@isgs.uiuc.edu; [4]Department of Civil and Environmental Engineering, University of Illinois, Urbana mrood@uiuc.edu

Abstract

This study describes a procedure of using grand canonical Monte Carlo simulations for structural characterization of single-walled carbon nanotube (SWNT) samples. Simulations of nitrogen adsorption were performed on the external and internal surface of homogenous arrays of SWNTs of diameters previously determined from Raman spectroscopy of the samples. The results showed the importance of peripheral grooves on a nanotube bundle and the insensitivity of nanotube diameter towards adsorption on the external surface of a bundle. Simulations also revealed that samples containing thin nanotubes would have less internal and more external adsorption than those comprising of large diameter nanotubes. The total adsorption inside nanotubes could be adjusted by a parameter (between 0 and 1) that resulted in a near perfect fit between simulated and experimental values. This parameter can be interpreted as the fraction of open-ended nanotubes in the sample.

I. Introduction

Several experimental studies have used gas adsorption as a standard technique to explore the fundamental adsorption properties of SWNTs. In general, the reported surface area of SWNTs ranges from 150 m^2/g to 1587 m^2/g, which depends on the adsorbate gas used for analyses and the specific structure and composition of the samples.[1] Most of these studies subjected nanotubes to oxidative purification processes that not only enhanced the purity of samples but also opened the ends of nanotubes.[1, 2] However, a precise quantification of open-ended nanotubes or direct evidence of cut nanotubes has not been completed[1] and typically all nanotubes are assumed open. To the best of our knowledge only Du et al. have described a rudimentary procedure for determining the relative amount of open-ended SWNTs in tested samples.[3] These researchers[3] used pore size distributions to determine that as-produced HiPco SWNTs[4, 5] contain as much as 40% open-ended nanotubes and purification processes reduce this value to negligible fractions.

The knowledge of open-ended nanotubes in a sample is essential to determine the amount of adsorption that would occur *inside* the nanotubes. The overall adsorption on SWNTs is a contribution from various adsorption sites. Due to strong van-der Waals interactions, SWNTs adhere to each other and form bundles or ropes and, thus, the adsorption sites are defined for the entire bundle as opposed to an individual nanotube.[6-9] There are four possible sites for adsorption: **1**, hollow interior of nanotubes; **2**, interstitial channels between the nanotubes; **3**, grooves present on the periphery of a nanotube bundle and **4**, the exterior surface of the outermost SWNTs (Figure 1).[6] Due to the structure of nanotubes, site **1** is the

most easily visualized adsorption site which would provide a large volume for adsorption and gas storage. However, unlike sites **2**, **3** and **4** that are available for adsorption on open and close-ended nanotubes, site **1** can only be accessed by nanotubes that are open-ended.

Figure 1. Four different adsorption sites on a homogeneous bundle of open-ended single-walled carbon nanotubes (SWNTs): (1) internal (endohedral), (2) interstitial channels, (3) external groove sites, and (4) external surface.
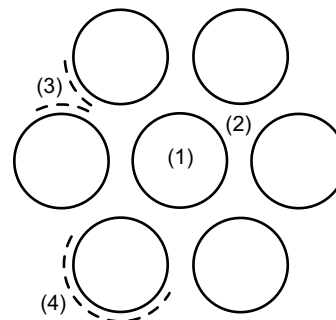
II. Experiments, Simulations and Analytical Methods

In this study, molecular simulations of nitrogen adsorption in SWNTs were carried out with results that were comparable to those of an experimental study.[10] The nitrogen adsorption capacity of bundles of open-ended nanotubes was calculated by grand canonical Monte Carlo (GCMC) simulations of the NPT ensemble. The diameters of nanotubes selected for calculations were the diameters obtained from Raman spectroscopy of the samples.[10] Simulations were performed to predict experimental nitrogen adsorption capacities of purified nanotube samples that contained some open-ended SWNTs. The experimental details are provided elsewhere[10] and a brief description of results is presented here for clarity. The SWNT samples tested were manufactured by electric-arc and HiPco chemical vapor deposition (CVD) method[4,5], and contained 95-98 wt% (EA95) and ~80 wt% SWNTs (CVD80), respectively. The diameter of nanotubes and their relative amounts were determined by Raman spectroscopy. Sample EA95 contained three different sized nanotubes with majority being 15.2 Å wide. Sample CVD80, on the other hand, was more heterogeneous. This sample contained nanotubes of five different sizes, most being 9.0 Å in diameter (Table 1). The nitrogen adsorption isotherms (10^{-6} < p/p_o < 0.99), BET surface areas (0.03 < p/p_o < 0.3), and total and micropore volumes of samples EA95 and CVD80 were determined by standard nitrogen adsorption (77 K) technique (Micromeritics ASAP 2010 surface area analyzer). The samples were sufficiently aged (sample age > 7 months) to minimize the impact of aging.[10]

Table 1. Morphology of SWNT samples.

| Sample | Wt% [1] | | Diameter (Å) [2] | Relative amount [2] |
	SWNTs	Impurities		
EA95	95 - 98	3 - 5	11.5	1.0
			14.0	2.3
			15.2	3.5
CVD80	~80	~20	9.0	4.3
			10.2	2.2
			10.7	1.7
			11.1	1.1
			11.8	1.0

[1] Manufacturer specified information; [2] Determined from Raman spectroscopy

In the molecular simulations reported here the nitrogen molecules were treated as structureless spherical particles which interact via dispersive forces only. Although the N_2 molecule has a quadrupole moment, it does not significantly change the simulated adsorption isotherm at 77 K. The interaction between N_2 molecules was modeled by the 12-6 Lennard-Jones potential

$$u_{ij}(r) = 4\varepsilon_{ij}\left[(\sigma_{ij}/r)^{12} - (\sigma_{ij}/r)^{6}\right] \tag{1}$$

(r is the intermolecular distance), as is the interaction between the carbon atoms of a nanotube and each N_2 molecule. The well depths ε_i/k_B, where k_B is Boltzmann constant, and collision diameters σ_i used are given in Table 2. The cross terms were obtained using the standard Lorenz-Berthelot combining rules: $\varepsilon_{ij} = \sqrt{\varepsilon_i\varepsilon_j}$ and $\sigma_{ij} = (\sigma_i + \sigma_j)/2$.

Table 2. Lennard-Jones potential parameters.

Site–site	ε/k_B (K)	σ (Å)
C–C	28.00	3.400
N_2–N_2	100.40	3.609

In order to simulate nitrogen adsorption in samples EA95 and CVD80, a simulation box that would contain a heterogeneous distribution of SWNTs would be the most appropriate structural arrangement of nanotubes. However, making heterogeneous nanotube bundles[8] that closely resemble the bundle size and the diameter distribution of experimental samples could be quite complicated because of which an alternative methodology was employed.

Simulations were performed on homogeneous arrays of SWNTs of diameters presented in Table 1. The positions of the individual carbon atoms in a nanotube were assumed unimportant at the temperatures of interest in this study, i.e. each nanotube in the bundle was considered to be a smooth structureless nanocylinder. At very low temperatures corrugation effects would become important. An effective potential was developed by integrating the C–N_2 potential over the positions of all carbon atoms in a tube of infinite length.

$$U_{sf}(\delta) = \frac{4R}{a_c}\int_0^{+\infty}\int_0^{\pi} u_{sf}(r)\ d\theta\ dz\,, \quad r^2 = R^2 + \delta^2 + z^2 - 2\delta R\cos\theta\,, \tag{2}$$

where U_{sf} is the interaction potential between a nitrogen molecule at a nearest distance δ from the axis of a nanotube of radius R; z is the distance along the tube axis (considered infinite); θ is the radial angle, and $a_c = 2.6185$ Å^2 is the surface area per carbon atom of the tube. By integrating over z and θ, Eq. (2) is reduced to a one-dimensional potential which depends on δ only.

The multi-dimensioned integral in Eq. (2) was numerically evaluated using the FORTRAN package QB01 from the Harwell Subroutine Library. Simpson's rule was selected as the integration method with a prescribed relative accuracy set to 10^{-5}. We noted that an analytical expression for the solid–fluid potential inside a cylindrical pore has been obtained by Tjatjopoulos et al. (1988) for spherical Lennard-Jones interactions. To accelerate the

calculation of $U_{\mathrm{sf}}(\delta)$, Eq. (2) was tabulated on a one-dimensional grid. For values of δ in the range $[0, R]$, the potential was tabulated on a grid with 31 equally-spaced knots in δ^2; for values of δ in the range $[R, 6.5R]$, the grid employed 56 equally spaced-knots in $1/\delta^2$. The potential was truncated at $\delta = 6.5R$. During the simulations, $U_{\mathrm{sf}}(\delta)$ was reconstructed from the tabulated information using cubic Hermite polynomial interpolation.

The simulations were carried out in two parts: adsorption on the external surface of a nanotube bundle (i.e., adsorption sites **3** and **4**), and adsorption inside the nanotube array (i.e., adsorption sites **1** and **2**). The inter-nanotube distance for all simulations was kept fixed at 3.4 Å (σ_s) to resemble nanotubes adhering to each other via van der Waals forces. Figure 2 shows the cross section, perpendicular to the tubes axis, of the unit simulation boxes employed in this work. The cross-sectional shape, identified by the shaded area, depends on the region of the nanotube bundle being probed. The box faces implement periodic boundary conditions, the two exceptions being the top face of the box in Fig. 2a, which is a reflecting wall, and the bottom one, which is blocked by the outermost shell of nanotubes in the bundle. The actual length of the simulation boxes was a function of the imposed sorbate pressure to keep an average number of molecules in the box greater than 50.

(a)

(b)
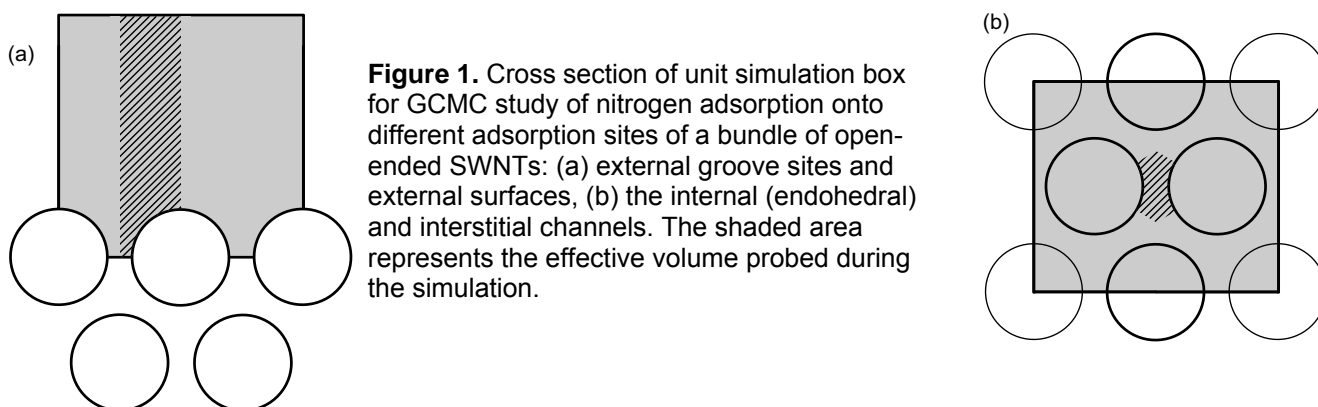
Figure 1. Cross section of unit simulation box for GCMC study of nitrogen adsorption onto different adsorption sites of a bundle of open-ended SWNTs: (a) external groove sites and external surfaces, (b) the internal (endohedral) and interstitial channels. The shaded area represents the effective volume probed during the simulation.

When simulating adsorption on the external surface of the bundle, a molecule was mapped onto the hatched area of Fig. 2(a) and interacted with the five nearest nanotubes depicted there (three on the outermost shell and two on the second shell). Including farther nanotubes had minimum impact on the total solid–fluid interaction potential. Notice that the nanotubes were not part of the simulation box and, therefore, molecules were not allowed to adsorb inside them. We also explored the alternative of making the outermost shell of nanotubes accessible for internal adsorption, and then correcting the final results by subtracting the average intratube adsorption from the total number of adsorbed molecules. Comparison of both methods showed that the external adsorption was not affected by intratube adsorption on the outermost shell. Figure 2(b) shows the cross section of the unit simulation box employed to study internal and interstitial adsorption. To calculate the solid–fluid interaction potential for a molecule located inside a nanotube of the bundle it suffices to sum over the interactions of the molecule with the confining tube and the six nearest neighbors. The corrugation effect of the neighbor tubes was very small and, for practical purposes, did not affect the cylindrical symmetry of the total interaction potential. The net effect

was that the potential curve for intratube adsorption in the bundle had the same shape as that for an isolated tube, though the well depth was deeper.

The GCMC simulations were carried out using established procedures. In normal GCMC, insertions are attempted uniformly throughout the volume of the simulation box. For nanotube bundles, however, it is known *a priori* that much of this volume is filled by carbon atoms of the nanotubes and is inaccessible to sorbate molecules. Furthermore, not all portions of the accessible space are equally favorable; there exist preferred regions in which sorbate molecules are localized. This information can be incorporated into a GCMC simulation if the insertions are not attempted randomly throughout the volume. This was achieved by using configurational-bias techniques.[11-14] Due to the bias introduced into the Monte Carlo insertion moves, the acceptance rules for insertions and deletions must be altered to ensure that microscopic reversibility is satisfied and that the GC ensemble is still correctly sampled. The method has been described in detail elsewhere.[15]

In this work one of the simplest biased GCMC schemes was employed. The method is a variation of one of the techniques proposed by Snurr et al.[16] in their simulation work of adsorption of aromatic hydrocarbons in silicalite. An insertion was performed as follows. A number, N_{trial}, of trial positions were randomly chosen throughout the simulation volume, V. For each point $j = 1, \ldots, N_{trial}$ we calculated the solid–fluid potential energy, $U_{sf}^{(j)}$, due to the interaction between a sorbate molecule placed at that point and the potential field of the nanotube array, as well as the corresponding Boltzmann factor, $\exp[-\beta U_{sf}^{(j)}]$, where $\beta = (k_B T)^{-1}$ and T is the system temperature. Out of the N_{trial} trial positions, one, denoted by i, was selected with a probability

$$P^{(i)} = W_{sf}^{-1} \exp[-\beta U_{sf}^{(i)}],\tag{3}$$

Where
$$W_{sf} = \sum_{j=1}^{N_{trial}} \exp[-\beta U_{sf}^{(j)}].\tag{4}$$

The insertion of the molecule at the selected trial position was accepted with probability

$$acc(N \to N+1) = \min\left\{1, \frac{W_{sf}}{N_{trial}} \frac{f\,V}{N+1} \beta \exp[-\beta \Delta U_{ff}]\right\},\tag{5}$$

where N is the number of molecules present before the attempted insertion, f is the imposed gas-phase fugacity, and $\Delta U_{ff} = U_{ff}(N+1) - \Delta U_{ff}(N)$ is the change in the total sorbate–sorbate contribution to the potential energy of the system due to the insertion. A deletion was performed by randomly choosing a molecule and calculating the potential energy, $U_{sf}^{(1)}$, due to its interaction with the nanotube bundle. $N_{trial} - 1$ trial positions were randomly chosen throughout the simulation volume and $U_{sf}^{(j)}$ was computed for each trial point $j = 2, \ldots, N_{trial}$, as well as the quantity

$$W_{sf} = \sum_{j=1}^{N_{trial}} \exp\left[-\beta U_{sf}^{(j)}\right]. \tag{6}$$

The deletion attempt was accepted with probability

$$acc(N \to N-1) = \min\left\{1, \frac{N_{trial}}{W_{sf}} \frac{N}{fV} \beta \exp\left[-\beta \Delta U_{ff}\right]\right\}, \tag{7}$$

where $\Delta U_{ff} = U_{ff}(N-1) - \Delta U_{ff}(N)$ is the change in the total sorbate–sorbate contribution to the potential energy of the system due to the molecule deletion.

Each simulation run was equilibrated for 10^4 Monte Carlo cycles, where each cycle consists of N attempts to translate a randomly selected molecule and $\max\{30, 0.3N\}$ attempts to create or delete a molecule with $N_{trial} = 100$. Here, N is the number of molecules in the box at the beginning of each cycle. The production periods consisted of 3×10^4 Monte Carlo cycles. The maximum displacement for translation in the simulation box was adjusted during the equilibration phase to give a 50% acceptance rate. Standard deviations of the ensemble averages were computed by breaking the production run into five blocks.

After simulating the external and internal adsorption capacities of homogenous nanotube bundles, the overall adsorption for a sample was determined by relative averaging (Eqs. 8 to10) of adsorption in bundles of nanotube sizes relevant to a particular sample (Table 1).

$$q_{sim}^s(p/p_o) = \frac{\sum_{D=sample}(q_{sim,D}^s(p/p_o) \times \phi_D)}{\sum_{D=sample}(\phi_D)} \tag{8}$$

$$q_{sim}^i(p/p_o) = \left(\frac{100-\eta}{100}\right) \times \frac{\sum_{D=sample}(q_{sim,D}^i(p/p_o) \times \phi_D)}{\sum_{D=sample}(\phi_D)} \tag{9}$$

$$q_{sim}^T(p/p_o) = S^P{}_{sim} \times q_{sim}^s(p/p_o) + q_{sim}^i(p/p_o) \tag{10}$$

where $q_{sim,D}^s(p/p_o)$ and $q_{sim,D}^i(p/p_o)$, respectively, are the simulated amounts adsorbed on the external surface and inside of a bundle of nanotubes of diameter, D and at a relative pressure, p/p$_o$; ϕ_D is the relative amount of nanotubes of diameter D in the sample (Table 1); η is the wt% impurities in the sample (Table 1); $S^P{}_{sim}$ is the external surface area of nanotubes in the sample (m^2 of nanotubes/g of sample); and $q_{Sim}^s(p/p_o)$, $q_{Sim}^i(p/p_o)$ and $q_{Sim}^T(p/p_o)$ are external adsorption, internal adsorption and total adsorption on the sample at p/p$_o$.

III. Results and Discussion

A. External Adsorption

Adsorption was observed at pressures as low as 10^{-6} p/p_o. At such pressures, some nitrogen molecules were noticed to adsorb on the external grooves sites. Adsorption continued on the grooves till they were saturated at about 10^{-4} p/p_o. Other researchers[12, 15] have also suggested the possibility of adsorption on site **3**. However, their results were based on speculations for justification of peaks observed at 4 – 5 Å region in the pore size distributions of their samples.[15] The results presented here support the speculation[15] that such peaks most likely arise from the adsorption on the external grooves of a nanotube bundle.

Figure 3. Snapshots of nitrogen molecules adsorbing on the surface of homogeneous SWNT bundles of tube diameter D = 9.0 Å (left) and D = 15.2 Å (right). p/p_o = 10^{-6} (a), 10^{-4} (b), 10^{-3} (c), 10^{-2} (d), 0.9 (e).
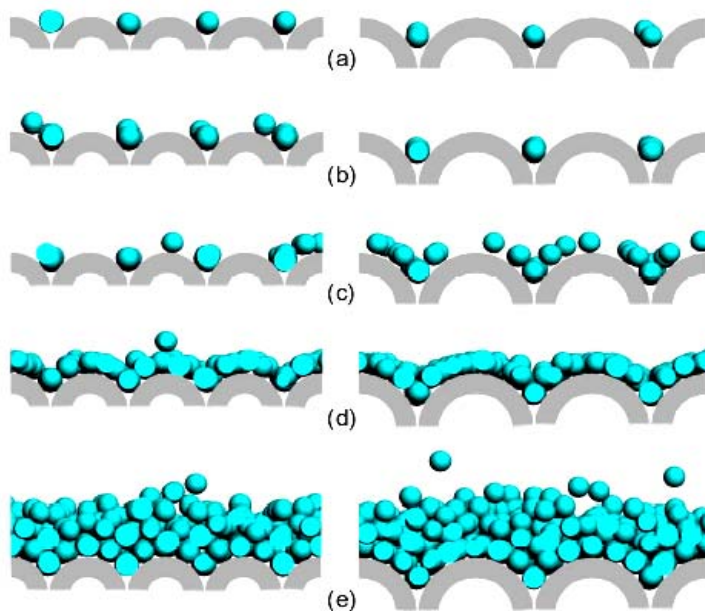
Increasing the vapor concentration above 10^{-4} p/p_o resulted in adsorption on the curved surface of the nanotubes (site **4**). At 10^{-3} p/p_o, partial coverage of the external surface was observed. Further increase in vapor concentration till 10^{-2} p/p_o resulted in complete monolayer formation following which adsorption proceeded rapidly with increasing vapor concentration. The mechanisms of nitrogen molecules adsorbing on the external surface of nanotubes are illustrated in Figure 3. It was also observed that the trends in external adsorption were independent of the nanotube size. Adsorption on an array of 15.2 Å diameter nanotubes proceeded in more or less the same fashion as that on 9.0 Å wide nanotube array, which showed that nanotube size has little or no effect on the total external adsorption capacity. The insensitivity of nanotube diameter towards the external adsorption capacity was evident from the isotherms (Figure 4). The adsorption capacity, as a function of p/p_o, was determined by calculating the amount adsorbed per unit external surface area of the bundle. The isotherms followed similar trends for all nanotube sizes with minimal but perceptible adsorption till ~10^{-3} p/p_o (< 10% of that at near saturation). The adsorption capacities of all arrays exhibited indistinguishable differences with respect to the nanotube diameter. Although, it appeared that at concentrations lower than 10^{-5} p/p_o, wider nanotubes had higher external adsorption capacities, the differences in absolute values of adsorption were too small to reach any such conclusion. Thus, it would be reasonable to say that adsorption on sites **3** and **4** is insensitive to the diameter of nanotubes.

Figure 4. Amount of nitrogen adsorbed on the surface of homogeneous bundles of nanotubes of diameters same as those in samples EA95 and CVD80.
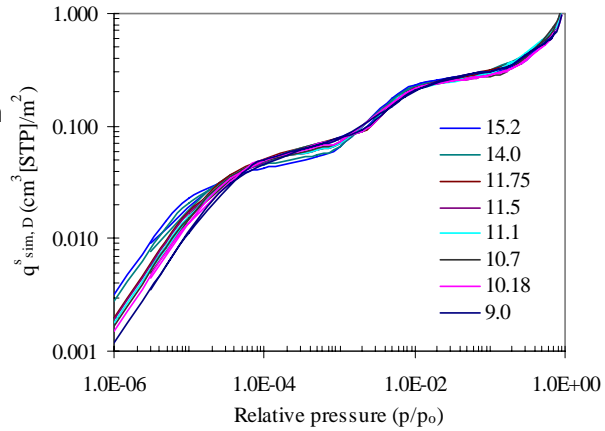
The external surface areas (i.e., S^P_{sim} in Eq. 10) of samples EA95 and CVD80 were determined by plotting the total experimental adsorption capacity of the samples (cm^3[STP]/g of sample) against the simulated amount adsorbed on the external surface of the bundle (cm^3[STP]/m^2 of nanotubes, Eq. 8), at same p/p_o (Figure 5). The plots are interpreted to comprise of two regions: the first region shows a steep rise and the second region that nearly follows a straight line. The first region of the curve indicates that the experimental adsorption capacity surpassed the simulated values, which means that internal adsorption in the sample was much higher than external adsorption. The second region of the curve implies that the experimental adsorption capacity was linearly proportional to the simulated external adsorption capacity or, in other words, majority of adsorption in the sample occurred on the external surface of the bundles. The slope of the second region of the curve, thus, represents the total external surface area of nanotubes in the sample. Additionally, the intercept of the straight line through the linear part of the curve provides the micropore volume of the sample because the amount adsorbed at zero surface loading is adsorbed entirely inside the pores. Furthermore, the relative pressure at the point of inflexion in the curve (i.e., meeting point of the two regions of the curve) is indicative of the maximum pressure above which the internal volume of nanotubes will be filled.

Figure 5. Total experimental adsorption capacity vs. simulated surface adsorption capacity for samples (a) EA95 and (b) CVD80. The slope and intercept of the straight line represents total external surface area of nanotubes and micropore volume of the samples.
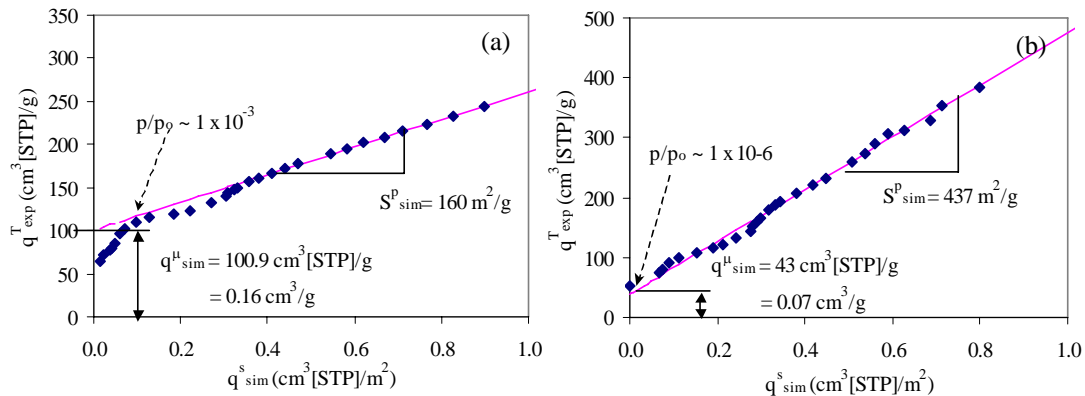
The total external surface area of nanotubes (S^P_{sim}) and the micropore volumes (q^μ_{sim}) of samples EA95 and CVD80, as calculated by the method described above, are presented in

Figure 5. The plots suggest that the micropores in sample EA95 will not be filled till 10^{-3} p/p$_o$ but those in sample CVD80 will be filled at the very beginning (10^{-3} p/p$_o$) of the isotherm. The total external area of sample CVD80 (437 m^2/g) was more than twice of that of sample EA95 (160 m^2/g), which indicated large quantities of small width bundles in sample CVD80. Comparison with experimental micropore volumes (Table 3) confirmed an excellent agreement with simulated micropore volumes (q^{μ}_{sim}) of the two samples. The total external surface areas, however, were different from the experimental values, with noticeable differences for sample CVD80.

B. Internal Adsorption

Simulations of nitrogen adsorption inside the nanotube array (henceforth, referred to as internal adsorption) revealed that the interstitial channels between neighboring nanotubes (site **2**) are generally not preferred for adsorption. However, single file adsorption of nitrogen molecules in site **2** was observed for arrays of 15.2 Å wide nanotubes (Figure 6), although significant adsorption in interstitial channels was observed only at comparatively high nitrogen pressures (> 10^{-4} p/p$_o$). The adsorption site **2** is essentially a channel the width of which depends on the size of nanotubes forming the channel and, as a result, the interstitial channels for large diameter nanotubes can be wide enough to accommodate a nitrogen molecule. This discussion, however, is less important, as actual nanotube bundles are heterogeneous with interstitial channels of various sizes some of which could be large enough to have unrestricted adsorption.[9] The internal adsorption isotherms of nanotube arrays indicated that as the nanotube size is increased from 9.0 Å to 15.2 Å, higher p/p$_o$ would be needed to saturate the bundles. Arrays of 9.0 Å nanotubes were nearly saturated at nitrogen pressures as low as 10^{-6} p/p$_o$, while those of 15.2 Å wide nanotubes could not be saturated till 10^{-3} p/p$_o$. Also, the adsorption capacity of 15.2 Å nanotube array (260 cm^3[STP]/g) was more than five times that of 9.0 Å nanotube array (52 cm^3[STP]/g). Thus, SWNT samples containing wide nanotubes would have large micropore volume that would be saturated at relatively higher nitrogen pressures.

Figure 6. Snapshots of nitrogen molecules adsorbed inside SWNT bundles of (a) 9.0 Å, (b) 11.5 Å, (c) 14.0 Å and (d) 15.2 Å nanotubes at p/p$_o$ ~ 0.9 and 77 K.
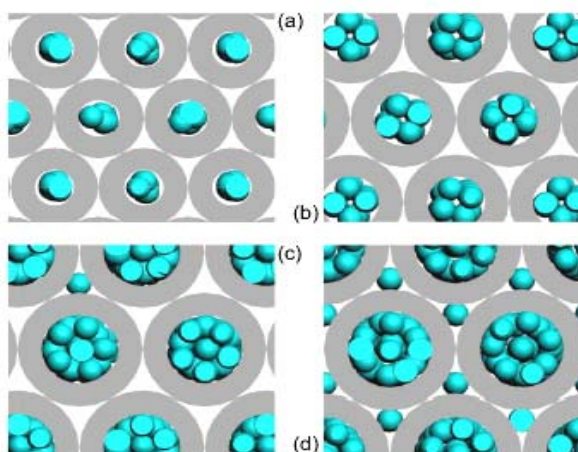
C. Total Adsorption

The total adsorption capacities of samples EA95 and CVD80, as determined from simulations, were calculated by summation of their internal and external adsorption capacities (Eq. 10). The adsorption isotherms are presented in Figure 7. The simulated isotherms were used to calculate the total surface area and the total pore volume of the samples. The

micropore volume of samples was determined from the maximum internal adsorption (Eq. 9). These values are presented in Table 3.

Figure 7. Simulated nitrogen adsorption capacity of SWNT samples (a) EA95 and (b) CVD80. Notice that due to a larger total external surface area, the external adsorption capacities of sample CVD80 are higher than those of sample EA95.
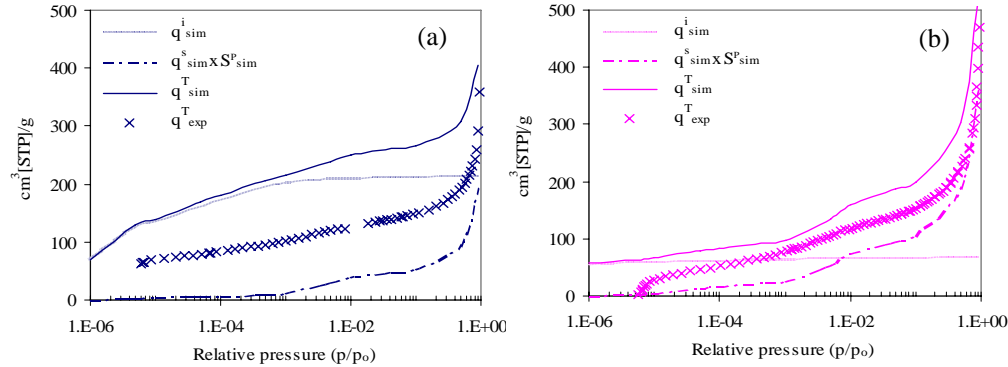
Table 3. Nitrogen adsorption surface area and pore volumes of samples EA95 and CVD80 as determined from simulations and experiments. T and Ex = total BET and external surface area. TP and μP are total and micropore volumes. Notice that the simulation values are the *maximum* achievable values for the two samples.

Sample	Simulation[1]				Experiments			
	Surface area (m^2/g)		Volume (cm^3/g)		Surface area (m^2/g)		Volume (cm^3/g)	
	T	Ex	TP^2	μP	T	Ex	TP^3	μP
EA95	1207	160	0.64	0.34	507	155	0.57	0.16
CVD80	892	437	0.84	0.11	609	339	0.92	0.07

[1]100% open nanotubes; [2]Calculated at 0.90 p/p_o; [3]Determined at 0.99 p/p_o

For sample EA95, $p/p_o \approx 10^{-3}$ appeared to be a critical point in the isotherm as the internal adsorption was saturated at $p/p_o \approx 10^{-3}$ and the external adsorption became significant at $p/p_o > 10^{-3}$. For sample CVD80, however, the internal adsorption was almost saturated at the beginning of the isotherm ($p/p_o \approx 10^{-6}$) and the external adsorption was significant at a much lower nitrogen concentration ($p/p_o \approx 10^{-5}$). These results were in compliance with the results presented in Figure 5. Also, at any given p/p_o, the internal adsorption was much higher and the external adsorption was much lower in sample EA95 than in sample CVD80. Additionally, the total surface area and micropore volume of sample EA95 (1207 m^2/g and 0.34 cm^3/g) were higher than the same for sample CVD80 (892 m^2/g and 0.11 cm^3/g). Thus, it can be concluded that samples containing large diameter nanotubes (EA95) would be more suitable for gas separation and storage than those containing thin nanotubes (CVD80). Comparison of simulated isotherms of both SWNT samples with experimental isotherms revealed two important points. First, the shape of simulated isotherms was similar to that of the experimental isotherms, which suggested that the methodology of calculating the adsorption isotherm (as a combination of external and internal adsorption in homogeneous bundles) was

most likely correct. Second, the adsorption capacities, total surface area, and total and micro pore volumes for simulated isotherms were much higher than the corresponding experimental values (Table 3), which suggested that the simulated values were highly idealized.

Until now, the calculations were carried out with an implicit assumption that all nanotubes were open and thus contribute to the internal and total adsorption. Consequently, the simulated isotherms presented in Figure 9 and the corresponding values of total surface area and pore volumes of samples EA95 and CVD80 (Table 3) are the *maximum* achievable values for these samples. In reality, however, only few nanotubes are open. If a more practical approach is to be taken then a factor describing the fraction of open-ended nanotubes should be incorporated in the calculations. This would alter the internal adsorption capacity of the bundles without affecting the external adsorption, as adsorption outside the bundles occurs for close-ended nanotubes. Thus, Eq. 10 would be modified to:

$$q_{sim}^{T}(p/p_{o}) = S_{sim}^{P} \times q_{sim}^{s}(p/p_{o}) + \upsilon \times q_{sim}^{i}(p/p_{o}) \tag{11}$$

The parameter υ is the fraction (between 0 and 1) of open-ended nanotubes of diameter D, and can be determined by trial-and-error to yield an isotherm that fits the experimental isotherm. Alternately, υ can also be calculated as the ratio of experimental micropore volume to the maximum simulated micropore volume.

$$\upsilon = \frac{\text{Experimental micropore volume}}{\text{Maximum micropore volume}} \tag{15}$$

Figure 8. Simulated nitrogen adsorption capacity of SWNT samples calculated by assuming (a) 45% open nanotubes in EA95 and (b) 60 % open nanotubes in CVD80. υ was estimated by trial-and-error method. Notice the near perfect replication of experimental isotherms.
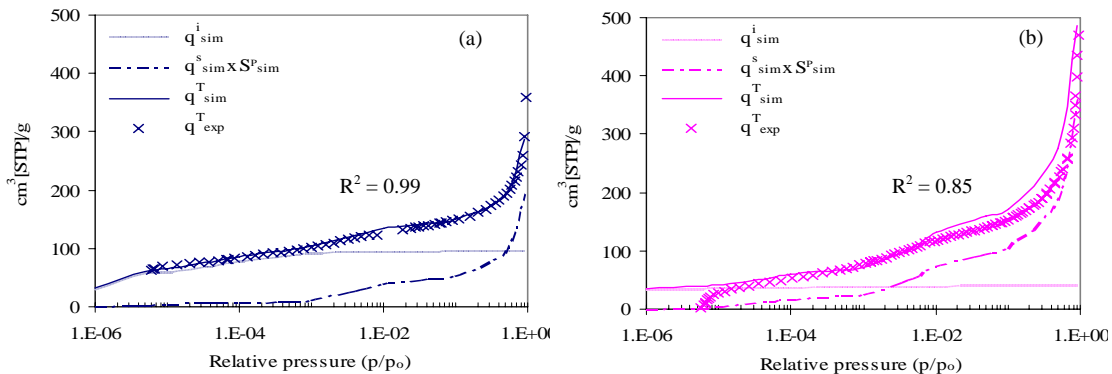
Adjusting υ to 0.45 and 0.60 for samples EA95 and CVD80, respectively, resulted in a near perfect fit between simulated and experimental isotherms (Figure 8). Also, the BET surface areas and the micropore volumes of sample EA95 closely agree with the experimental values (Table 3). The micropore volumes were also comparable to the q_{sat}^{μ} values as calculated in Figure 5. Sample CVD80, however, does not exhibit a closure between simulated and experimental values which is believed to be due to relatively large quantities of impurities present in the sample. Overall, it can be said that samples EA95 and CVD80 contained 45% and 60% open-ended nanotubes, respectively.

IV. Summary and Conclusions

This study describes a procedure of combining grand canonical Monte Carlo simulations of SWNTs with experimental characterization of actual nanotube samples. Simulations were performed to determine the nitrogen adsorption capacity on the external and internal surface of homogenous arrays of SWNTs of diameters determined from the Raman analysis of samples.[15] Adsorption on the grooves present on the periphery of a nanotube bundle was observed at vapor concentrations as low as 1×10^{-6} p/p_o with total external adsorption being independent of the nanotube size and being equivalent to that of a homogenous bundle of 12.12 Å wide nanotubes. The internal adsorption isotherms of nanotube arrays indicated that adsorption in the interstitial channels between nanotubes can occur in homogenous arrays of wide nanotubes, and the amount of nitrogen adsorbed and the p/p_o needed to saturate the bundles increases with increasing nanotube size. Comparison with experimental values suggested that adjusting the total adsorption inside the nanotubes could result in a near perfect fit between simulated and experimental values for both samples. This factor can be interpreted as the fraction of open-ended nanotubes in the sample. This analysis showed that samples EA95 and CVD80 that were tested in a previous study[15] contained only 45 % and 60 % open-ended nanotubes, respectively, and their surface areas can be increased from 507 m^2/g and 609 m^2/g, respectively, to a maximum of 1207 m^2/g and 892 m^2/g.

References

1. Cinke M, Li J, Chen B, Cassell A, Delzeit L, Han, J et al. Chem Phys Lett 2002; 365(1):69-74.
2. Fujiwara A, Ishji K, Suematsu H, Kataura H, et al. Chem Phys Lett 2001; 336(3):205-211.
3. Du W, Wilson L, Ripmeester J, Dutrisac R, Simard B, et al., Nano letters 2002; 2(4):343-346.
4. Nikolaev P, Bronikowski MJ, Bradley RK, Rohmund F, et al. Chem Phys Lett 1999; 313(1):91-97.
5. Bronikowski MJ, Willis PA, Colbert DT, Smalley RE. J Vac Sci Technol, A 2001; 19(4):1800-1805.
6. Zhao J, Buldum A, Han J, Lu JP. Nanotechnology 2002; 13(2):195-200.
7. Du W, Wilson L, Ripmeester J, Dutrisac R, Simard B, et al., Nano letters 2002; 2(4):343-346.
8. Talapatra S, Zambano AZ, Weber SE, Migone AD. Phys Rev Lett 2000, 85(1):138-141.
9. Shi W, Johnson JK. Phys Rev Lett 2003, 91(1):015504-4.
10. Agnihotri, S., Rostam-Abadi, M., Rood, M.J. Carbon 2004, 42 (12-13): 2699-2710.
11. Siepmann, J. I. Mol. Phys. 1990, 70, 1145.
12. Siepmann, J. I.; Frenkel, D. Mol. Phys. 1992, 75, 59.
13. Frenkel, D.; Mooij, G. C. A. M.; Smit, B. J. Phys.: Condens. Matter 1992, 4, 3053.
14. de Pablo, J. J.; Laso, M.; Sutter, U. W. J. Chem. Phys. 1992, 96, 2395.
15. Frenkel, D.; Smit, B. Understanding Molecular Simulation (Academic Press, London, 1996).
16. Snurr, R. Q.; Bell, A. T.; Theodorou, D. N. J. Phys. Chem. 1999, 97, 13742.